

Development of a Retinal Image Segmentation Algorithm for the Identifying Prevalence Markers of Diabetic Retinopathy Using a Neural Network

Muluneh Hailu Heyi

Department of Electrical and Computer Engineering,
Hawassa University,
Hawassa, Ethiopia,

Daniel Moges Tadesse

Department of Biomedical Engineering,
Hawassa University,
Hawassa, Ethiopia,

Abstract:- Diabetic Retinopathy (DR) is a prominent cause of blindness and visual problem that affects the eyes of humans who are affected by diabetics. Most of the time it does not show symptoms at an early stage and it is hard for the patient to identify the symptoms until a visual ability degrade and the treatment becomes is less effective. It becomes tough for medical experts (ophthalmologists) to identify DR at an early stage manually by observing the retinal image taken by a fundus camera. Thus, computer-aided image processing of retinal images taken by fundus camera has tremendous advantages to detect retinal lesions associated with Diabetic Retinopathy at an early stage. With less time and effort, the computer aid image processing examines a large number of images more accurately than the manual observer-driven techniques. It becomes important diagnostic aid to reduce the workload of ophthalmologists. However, the presence of various artifacts like the similarity of anatomical structures, movement of the patient eye during image capturing, device noise, and illumination makes the segmentation and processing of images of major pathological structures a difficult task.

In this study, we have developed a retinal image segmentation algorithm and user-friendly software that can ease the task of the medical experts by automatically identifying Hard Exudates (HEs), which are the most prevalent characteristic features of Diabetic Retinopathy in its earliest stage. The algorithm first is written and tested using MATLAB then user-friendly software is developed using C# programming language in the Microsoft .Net framework. To classify and segment the retinal image taken by the fundus camera a general representation of images color in the three spaces (trinion) has been used and to extract image features a trinion based Fourier Transforms has also been applied. Neural Network (NN) based segmentation of Hard Exudates are included in the method for color space transformation and to extract features.

The efficiency of the developed image processing has been tested in classifying and identifying hard exudated and it shows better results.

Keywords:- Retinal Imaging, Image Processing, Image Segmentation, Neural Network, Diabetic Retinopathy.

I. INTRODUCTION

The human eye has many parts which have their purposes and to process the interior image of an eye needs a better understanding of the parts. The retina acts like the film of the eye on the interior surface of the human eye and is used to change light rays into electrical signals. Through optical nerves, it sends converted electrical signals to the brain. The optic nerve act as a wire to connect the eye with the brain for the electrical signal. The optic disc (OD) is the small round mark on the retina where the optic nerve exits and the blood vessels enter the eye, and it has a lighter area on the retina image. The macula is found around the central region of the retina which is used to control the central light vision. The fovea is a small part of the retina found in the center of the macula which is responsible for the highest visual acuity. The vascular network is a network responsible for providing oxygen, nutrients, and blood to the retina (Afzal 2003).

The human eyes will lose their sight due to different reasons and Diabetic Retinopathy (DR) is one of them. Diabetic Retinopathy (DR) is a prominent cause of blindness and visual problem that affects the eyes of humans who are affected by diabetics. Most of the time it does not show symptoms at an early stage and it is hard for the patient to identify the symptoms until a visual ability degrade and the treatment becomes is less effective. It becomes tough for medical experts (ophthalmologists) to identify DR at an early stage manually by observing the retinal image taken by a fundus camera. Diabetic Retinopathy (DR) has different forms and stages to affect eye vision and these stages are represented by the characteristic features of DR which are: Microaneurysms (MA), Hemorrhages (H), and Exudates (Hard Exudates (HE) and Soft Exudates (SE)). MA are discrete, localized expansions of weakened capillary walls and show up as small, red 'dots' on the retina. When the small blood vessels rupture, bleeding occurs over time. They generally appear as either a red 'dot' or 'flame-like' on the retina. Exudates are the main sign of DR, a common retinal complication related to diabetes and the leading cause of blindness. Hard exudates (HEs) are the most specific markers for the presence of retinal edema, the major cause of vision loss in nonproliferative forms of DR, and one of the most

common lesions in the early stages of DR (Phillips et al. 1993). HE is caused by the leakage of proteins and lipids from the blood into the retina through damaged blood vessels. They appear as white or yellow patches in retinal images, sometimes as ring structures around leaking capillaries. As the severity of DR in the blood progresses, the vessels become clogged, leading to a micro-infarct in the retina called SE. In advanced stages, this leads to diabetic macular edema (DME).

DR is not a curable disease, but if it is sensed in the early stages major vision loss can prevent with laser treatment. This is why diabetics need to have regular fundus camera examinations of the back of their eyes. A variety of

ophthalmoscopic techniques, including digital fundus photography, indirect ophthalmoscopy, stereoscopic biomicroscopy, fluorescence angiography, and optical coherence tomography (OCT), are used for the diagnosis and treatment of ophthalmic diseases. However, due to their relatively low cost, simplicity, and accessibility, fundus cameras are the most commonly used. 2D imaging of translucent 3D retinal tissue is suitable for observing fundus and structures (see Fig 1). Most commonly used to identify and assess symptoms of retinal detachment or ocular disease due to DR. Color images of the fundus of the eye are also taken to document the presence of disease and to observe its change over time.

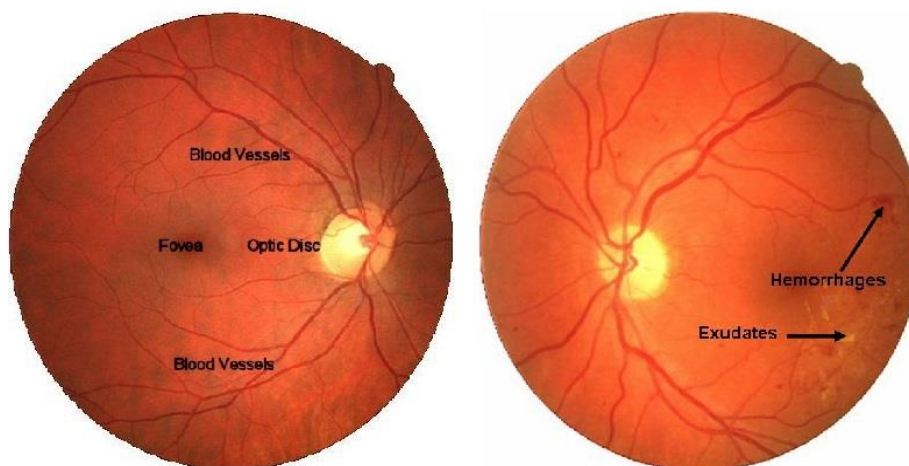


Fig. 1. RGB-colored retinal Image was taken by fundus (Osareh and Shadgar 2009).

The main objective of the study was to develop an automated method for processing retinal images based on an image captured by a fundus camera, which would allow effective detection and mass screening of DR markers. This research paper explains the holistic approach to retinal image analysis, texture feature extraction for detection of HE, signature map created to enhance EXs, and OD, classification used to identify abnormal retinal images, and development of user-friendly software that allows medical experts to easily operate the system.

II. RELATED WORKS

The authors (Satya et al. 2019) proposed an algorithm to detect HEs using morphological operations. Their algorithm consists of three stages: First, preprocessing, second, feature extraction, and third, HEs detection. They apply contrast enhancement and noise removal to the green component of the retinal color image, and only this channel is used for further analysis. In the second phase, features are extracted to detect the candidates of HE using morphological operations (top-hat and bottom-hat). Finally, the algorithm detects HEs by finding the difference between the bottom-hat and top-hat features. To investigate their proposed algorithm, they used the DIARETDB1 and the High-Resolution Fundus (HRF) image database. Using the DIARETDB1 database, they achieved an average sensitivity of 94%, a specificity of 96%, and an accuracy of 95%. With the HRF retina database, they

attained an average sensitivity of 95%, specificity of 95%, and accuracy of 97%.

The authors (Shengchun et al. 2019) also proposed an algorithm to detect HEs. First, they perform an automatic preprocessing method for retinal images by using the active thresholding technique and the fuzzy Cmeans clustering (FCM) technique, and then use a classifier called Support Vector Machine. Their proposed algorithm includes four stages. The first stage is preprocessing, the second is optic nerve head localization, the third stage is determining the eligible HEs by using a dynamic threshold in clustering with a global threshold based on FCM, and the last stage is feature extraction. In the last stage, the eight texture features were extracted from the candidate regions, which were then fed into an SVM classifier for automatic classification of HEs. DIARETDB1 and the retinal image database eophtha EX were used to try to evaluate the algorithm. Trained and cross-validated at the pixel level (10 times) using the eophtha EX and DIARETDB1 retinal databases. Mean sensitivities of 76.5%, PPV of 82.7%, and Fscore of 76.7% were achieved using eophtha EX archives and using the DIARETDB1 retinal database. Average sensitivity of 97.5%, specificity of 97.8% and accuracy of 97.7%.

(Anup et al. 2017) have proposed an algorithm for feature-based classification of HE in retinal images. First, each of the three color components is preprocessed, then the optic disk and blood vessels are extracted from the image and

finally the exudate pixels on the image are identified/classified using region growing technique. They have used standard retinal image databases and achieved an average accuracy of 99% in segmenting or classifying HE pixels in an image. (Vikram et al. 2020) have also proposed a neural network-based method for diagnosis of DR -related diseases.

(SHILPA et al. 2018) have proposed an algorithm for detecting HEs. Their proposed algorithm includes three stages: the first is preprocessing, the second is morphological operation, and the third stage is segmentation of HEs. They apply the morphological reconstruction to the green component of the retinal color image. In the second stage, features are extracted to detect the candidates HE using the morphological operation. The final segmentation algorithm recognizes the HEs considering their features.

In a literature review, many researchers have developed various methods for segmenting HE, vascular, fossa, and external diameters in fundus images (Eadgahi and Pourreza 2012, Niemeijer et al. 2007, Ehsan and Somayeh 2012, Liu et al. 2008 and Godse et al. al., 2013). In general, most attempts at color fundus imaging have focused on analyzing each color component sequentially and combining results from different channels. However, these sequential methods hide the existing cross-correlations between color channels, and the associated computational costs are often high. In this regard, a more holistic approach to presentation and analysis can have tremendous benefits. A recent application of multidimensional algebra in color image analysis uses vector representations of the three color components in quaternion and trinion spaces. The corresponding integral transform allows analysis to be performed as a whole or as an entity while retaining information about cross-correlation (Assefa et al. 2010a and Assefa et al. 2011). Based on such a vectorial principle, in this study, we have developed a method for designing a robust retinal image segmentation algorithm that facilitates the task of medical experts to automatically identify HEs.

III. MATERIALS AND METHODS

1.1 Image Data Set

For analyzing the proposed image processing schemes a set of the color retinal images generated by fundus camera is collected from the Black Lion Hospital Diabetic Centre (in Ethiopia) (a total of 66 images), and standard retinal image data sets (a total of 393 images from 5 standard retinal image data sets).

For standard retinal image, the following publicly available standard retinal image data sets archives have been used for the developed algorithm performance evaluation, analysis, and testing. These datasets are DIARETDB0, DIARETDB1, High-Resolution Fundus (HRF) image database, STARE (STructured Analysis of the REtinal image) database and DRIVE (Digital Retinal Image for Vessel Extraction) dataset. From each database both normal and abnormal retinal images have been used.

The above publicly available archives consist of high-quality images with useful medical findings. Expert delineations are used as the gold standard for performance evaluation and comparison of different segmentation methods.

To evaluate the different situations and to produce robust image processing algorithms, we have tried to include the following types of retinal images in image data sets.

- Normal retinal images
- Retinal images with mild and moderate nonproliferative DR, which have HE, SE, MA, and H on them.
- Retinal images with glaucoma.

1.2 Image Analysis Methodology

The suggested method analyses color retinal images captured with digital fundus cameras from individuals with DR using a mathematical framework. It extracts important imaging features for classification and segmentation of retinal pictures using a general representation of color images in three-dimensional space and trinion-based Fourier transforms. The technique includes a suitable color space transformation and a method for extracting robust higher-order features, followed by HE segmentation using a Neural Network (NN). The efficacy of picture segmentation algorithms based on NN and Neuro Fuzzy (NF) in detecting the existence of major abnormality markers (HEs, SEs, MA, H) and attenuating intra an interimage fluctuations due to undesirable artifacts is comprehensively studied. The technique has been used to analyse images from a variety of typical retinal image data set, with encouraging results. The proposed methodology as shown in Fig.2, concentrates on the following two issues:

- Based on feature maps developed by extracting robust texture descriptors, effective augmentation of EXs, the OD, blood vessels, and other background structures.
- EXs are accurately segmented using a neural network (NN)-based classifier that has been created.

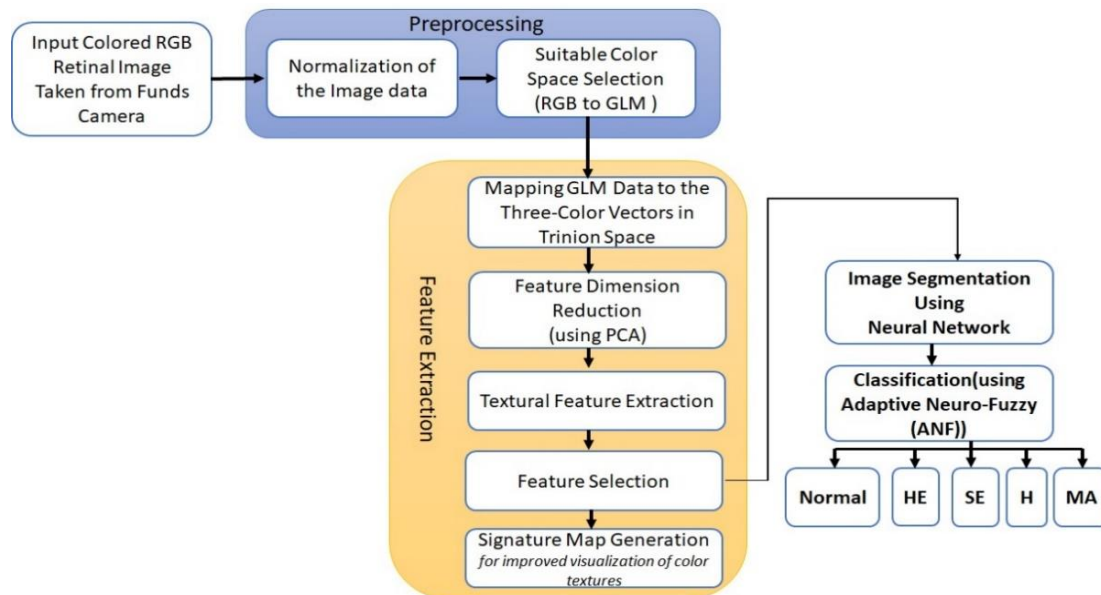


Fig. 2. The suggested image processing framework is depicted as a block diagram.

IV. IMAGE PROCESSING ALGORITHM DEVELOPMENT AND IMPLEMENTATION

Retinal Image processing has series of steps from holistic processing to feature extraction and NN. Hereunder we explain each phase of the image processing algorithm step by step.

1.3 Preprocessing

In the pre-processing phase, we have performed normalization of the image data and suitable color space selection. After the retinal image is read or loaded from the storage, the image data type is converted from unit8 to double. Then each color component is divided by 255 and their value becomes between 0 and 1. This image normalization process is applied to reduce the overflow error due to further analysis.

When the normalization process is completed appropriate color space must be selected. Because of retinal pigmentation and the acquisition process, retinal images vary greatly in brightness and contrast. This makes it more difficult to distinguish retinal features and lesions, which hinders automatic segmentation of abnormalities such as EXs.

Determining the color space that sends dominant light to the retina in an ideal way than the original RGB color space has proven useful for in-depth exploration. To this end, several color spaces such as RGB, HSL, Lab, LUV, CMYK, and Ycrbrr were tested and compared to their suitability for extracting highlights (surface descriptors) in a powerful and valuable way.

In a normal retinal image, the red component is oversaturated, resulting in low contrast in bright areas. The blue component is less saturated and the black areas has less contrast. A single green component enhances the contrast of the entire area. As a result, the image has very low contrast,

as large peaks are grouped together in small areas of the histogram.

For further analysis, two color spaces were selected and tested for better contrast and uniformity for EX and other retinal structures. HSL (Hue, Saturation, Brightness/Value/Intensity) and GLM (RGB G Component, LUV L Component, and CMYK Inverse Magenta Component). The first HSL color space was chosen because it is similar to human color perception and causes less variation within and between images due to various artifacts, potentially useful for our anomaly detection system. The second GLM color space was chosen based on the results of the scattering matrix of maximum interclass separability in (Lu and Fang G 2013). GLM color bars are important for improving DR performance.

As mentioned earlier, when using an image processing program to inspect DR, the green channel of the original color fundus image is typically used. The reason for this is that most methods rely on color intensity information as the basis for developing image processing algorithms for color images. The green channel of the fundus retinal image is often used for HE detection and segmentation due to the high contrast of HE (Snchez et al. 2009). However, a more holistic analysis is generally more meaningful and should therefore lead to a more effective analysis of color images. In this regard, the current work is a combination of three typical channels for anomaly detection based on DR and OD localization of fundus images. The G channel from the RGB color space was chosen based on the above facts. HE appears brighter in the fundus image than in the background, which is dominated by green channels. Due to the consistent EX and OD luminance information, the L channel in the LUV color space was chosen as the second channel (Kande et al. 2009). In most fundus images, the background color is red, while HE is yellowish. The inverse magenta channel from the CMYK color space was selected as the third channel. This is to allow good separation of dark red blood vessels from OD (see, for example, Figure 3). The GLM color space scatter matrix

calculated in (Lu and Fang G 2013) is larger than the RGB, HSV, LUV, and Lab color space scatter matrices in terms of separating EX from non-EX pixels.

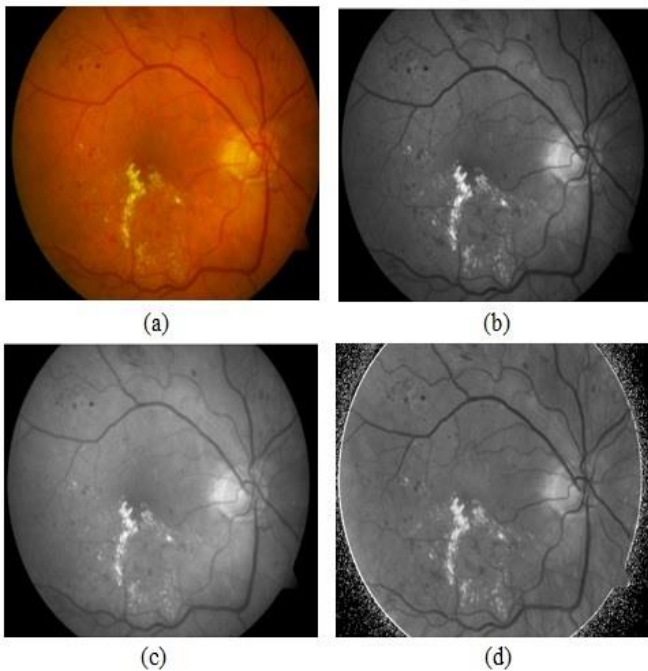


Fig. 3. (a)Sample original image, (b)green channel, (c)luminance channel, and

1.4 Feature Extraction

After the preprocessing phase is completed, the next phase is feature extraction which includes the following tasks:

- Mapping GLM’ data to the three-color vectors in Trinion space
- Feature Dimension Reduction
- Textural feature extraction for candidate detection and improved visualization
- Signature map generation

4.2.1. Mapping GLM’ data to the three-color vectors in Trinion space

The converted RGB color retinal image is mapped to Trinion as $H(x, y) = G + iL + jM$. We then performed a spatially localized analysis in the selected color space by calculating the Trinion-Fourier transform (TFT) in a 3x3 translation window.

Two practical definitions of the Trinion-Fourier transform (TFT) have been proposed (Assefa et al. 2011). The TFT of type I and vice versa (ITFT) are given by:

$$T(u,v) = \int_{-\infty}^{\infty} \int_{-\infty}^{\infty} h(x,y) (\cos(2\pi(ux + vy)) - \mu_1 \sin(2\pi(ux + vy))) dx dy \tag{1}$$

$$h(x,y) = \int_{-\infty}^{\infty} \int_{-\infty}^{\infty} T(u,v) (\cos(2\pi(ux + vy)) + \mu_2 \sin(2\pi(ux + vy))) dudv \tag{2}$$

Where $h(x, y)$ is generally an image function of the trinion value, μ_1 is a pure unit trinion, and μ_2 is a trinion, so

the product $\mu_1\mu_2 = -1$. The choice between μ_1 and μ_2 is optional. Similarly, to the previous studies (Assefa, et al., 2011), the choices of μ_1 and μ_2 are given by $\mu_1 = \frac{(i-j)}{\sqrt{2}}$ and $\mu_2 = \frac{(-1-i+j)}{\sqrt{2}}$.

Based on this the discrete TFT and its inverse are computed as follows:

$$T(u, v) = \frac{1}{MN} \sum_{x=0}^{M-1} \sum_{y=0}^{N-1} h(x, y) \left(\cos \left(2\pi \left(\frac{ux}{M} + \frac{vy}{N} \right) \right) - \mu_1 \sin \left(2\pi \left(\frac{ux}{M} + \frac{vy}{N} \right) \right) \right) \tag{3}$$

$$h(x, y) = \sum_{u=0}^{M-1} \sum_{v=0}^{N-1} T(u, v) \left(\cos \left(2\pi \left(\frac{ux}{M} + \frac{vy}{N} \right) \right) + \mu_2 \sin \left(2\pi \left(\frac{ux}{M} + \frac{vy}{N} \right) \right) \right) \tag{4}$$

Where:

$M \times N$ is the total number of voxels (vectors) found in the selected region of interest (window) of the source image. $u=0 \dots N-1, v=1 \dots M-1$, are the discrete frequencies along with the horizontal and vertical directions respectively.

4.2.2. Feature Dimension Reduction

Principal component analysis (PCA) was applied to each locally transformed 3×3 TFT image, each resulting in the output of the trinion value in the new PCA space, each image being formed from a 3×3 matrix in our case. This step is necessary to reduce some redundancy in our multichannel data. Then each value of the resulting 3×3 matrix is normalized from 0 to 1 and these are the probability density functions used to calculate the properties of the texture.

4.2.3. Extract texture features for candidate detection and image enhancement

Nine different Haralick texture features (Assefa et al. 2010a) were calculated: Sum Mean, Variance, Energy (Angular Second Moment), Correlation, Homogeneity, Contrast, Entropy, Cluster Shadow and Cluster Prominence and have been tested for their effectiveness in the quantification of different subjects. in our retinal samples. Each texture feature is extracted as a component of the PCA matrix with three values. The computed characteristic is then assigned to the centre value of the voxel in this window. This step is then repeated for all voxels contained in the selected region of interest in the image.

The above textural features were computed as follows:

$$Sum\text{-}mean = 0.5 \sum_{u=1}^3 \sum_{v=1}^3 (u p(u, v) + v p(u, v)) \tag{5}$$

$$Variance = 0.5 \sum_{u=1}^3 \sum_{v=1}^3 [(u - \mu)^2 p(u, v) + (v - \mu)^2 p(u, v)]$$

$$Energy = \sum_{u=1}^3 \sum_{v=1}^3 p(u, v)^2 \tag{7}$$

$$Correlation = \sum_{u=1}^3 \sum_{v=1}^3 \frac{(u - \mu_x)(v - \mu_y)p(u, v)}{\sigma_x \sigma_y} \tag{8}$$

$$Homogeneity = \sum_{u=1}^3 \sum_{v=1}^3 \frac{p(u,v)}{1+(u-v)^2} \tag{9}$$

$$Contrast = \sum_{u=1}^3 \sum_{v=1}^3 (u-v)^2 \log(p(u,v)) \tag{10}$$

$$Entropy = - \sum_{u=1}^3 \sum_{v=1}^3 p(u,v) \log(p(u,v)) \tag{11}$$

$$Cluster \quad shade = \sum_{u=1}^3 \sum_{v=1}^3 (u+v-\mu_x-\mu_y)^3 p(u,v) \tag{12}$$

$$Cluster \quad prominence = \sum_{u=1}^3 \sum_{v=1}^3 (u+v-\mu_x-\mu_y)^4 p(u,v) \tag{13}$$

Where:

$p(u,v)$ is the normalized spectral value (which can be thought of as a function of probability density) obtained after applying PCA to the TFT-transformed image matrix.

$\mu = \frac{1}{9} \sum_{u=1}^3 \sum_{v=1}^3 p(u,v)$ is mean of the matrix
 $\mu_x = \sum_{u=1}^3 u \sum_{v=1}^3 p(u,v)$ is the sum of row means,
 $\mu_y = \sum_{v=1}^3 v \sum_{u=1}^3 p(u,v)$ is the sum of column means,
 $\sigma_x^2 = \sum_{u=1}^3 (u-\mu_x)^2 \sum_{v=1}^3 p(u,v)$ is the sum of row variance, and
 $\sigma_y^2 = \sum_{v=1}^3 (v-\mu_y)^2 \sum_{u=1}^3 p(u,v)$ is the sum of column variance.

4.2.4. Signature map generation

The above feature values are normalized and used to create the final signature map. This allows you to distinguish between areas that correspond to other areas of clinical significance associated with HE, OD, and DR. The final result of the signature map was generated as a color using a 3-level local texture descriptor. The performance of signature maps generated by the various texture features was compared and evaluated accordingly by qualitative and quantitative comparisons between the signature maps and the available ground truths.

1.5 Image segmentation

To differentiate the HE from the normal part of the retinal image, the image resulted from the feature extraction process divided or segmented in to different regions based on the characteristic of pixels to identify the infected place. There are different techniques for image segmentation but due to its efficiency we used feed forward back propagating neural network to segment HE.

We have used the following specification to segment the image using Feed Forward Back Propagating Neural Network:

1. As shown in the Fig. 4, we have developed a NN which have 3 layers. The first layer/input layer contains three neurons, which is equal to the number of input feature vectors for the NN. In the second layer/ the hidden layer, we have used five neurons. The third layer/output layer contains one neuron which is equal to the number of output vector for the classifier.

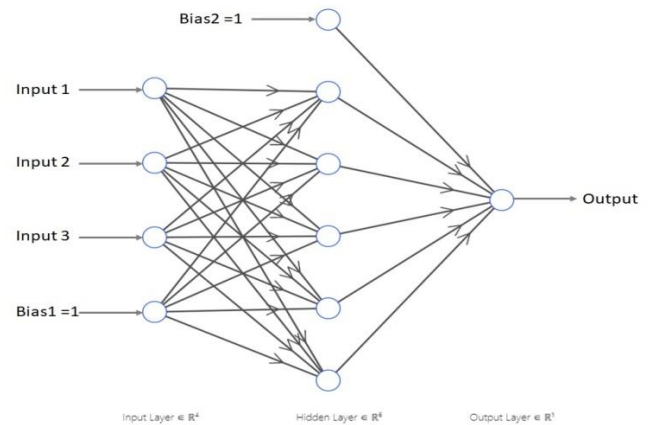


Fig. 4 the developed feed-forward back-propagating neural network

2. We have used the tan sigmoid activation function for all neurons in the hidden layer and linear activation function for the output neuron.
3. We have used a learning rate and moment values of 0.01 and 0.0071 respectively for all the neurons in the output and hidden layers. These parameter values are chosen after various testing and validation stages of the NN.
4. We have used the 1000 number of iterations. This parameter value is chosen after looking at the sum mean square errors of the validation, testing, and early training data sets.
5. We have used a total of 257000 training data set where each training data contains three features that are found in the signature map generation phase. The training data sets are manually selected from different structural positions of various images and it contains various normal retinal structures, and other structures with a symptom of mild non-proliferative DR, that have HE, SE, MA, and H on them. The training data set contains:
 - 64500 voxels (Feature vectors) of HE from different images,
 - 53400 voxels (Feature vectors) of SE from different images,
 - 50800 voxels (Feature vectors) of H from different images, and spatial positions
 - 12000voxels (Feature vectors) of MA from different images,
 - 76300 voxels (Feature vectors) of normal anatomical areas from different images, spatial positions, and structures
6. To decide the stopping point of iterations/number of epochs, and tune the NN parameters the total learning data set is first divided into three separate categories. These are the training, validating, and testing data sets where each of them contains a total of 112400,112400, and 32200 Voxels (Feature vectors) respectively. After assessing the results, the best performing NN parameters and number of epochs are chosen. Then the NN is trained and its training error is measured and compared with the testing error. The final training and testing mean square error results of the trained NN are in an acceptable range in iteration number 1000. Based on this we use the final trained NN to be used as a pixel-based HE classifier for a new feature.

After the image segmentation of HE is implemented using feed forward back propagating neural network, we have also developed a six-layer adaptive neuro-fuzzy (ANF) network to see its efficacy in classifying HE, SE, H, and MA, which are the most characteristic features of DR. In the six layer adaptive neuro-fuzzy network we have developed, the first layer is the input layer and it has three neurons each accepting the input vector. The second is the membership function layer and it has nine neurons, where each of them fuzzified each input based on the membership function parameters of each class. And the next third layer is the rule base layer and it has 27 neurons. The fourth layer is the normalized rule base layer and it has 108 neurons. Layer five is the defuzzification layer and it has 108 neurons. In this layer, there are 4 by 108 defuzzification parameters (learning capable weights and the product of the weights with the input vector gives defuzzification output when multiplied by the fired normalized rule base. The final layer is the output layer and it has four neurons for each output variable. It calculates the exact crisp output for each variable based on calculating the weighted sum of each fired and defuzzied rule. In the forward pass rule, consequent parameters are obtained based on given inputs and membership function parameters. In the backward pass, the antecedent parameters are updated based on the error found in the output layer.

V. PERFORMANCE ANALYSIS OF THE ALGORITHM

The methods used at each phase of the retinal image processing must be evaluated and analyzed to see its performance. At the preprocessing stage different analysis has been to select the best optimal feature map for segmentation of retinal images. The performance of signature map analyzed at the feature extraction phase and then performance NN in segmenting HEs is evaluated.

1.6 Evaluation of the optimal feature map selection for retinal image segmentation

Quantitative analysis of the available baseline data revealed that signature maps were generated based on three characteristics: cluster prominence, mean sum and variance calculated in GLM and HSV color spaces, superior to other features in its ability to clearly identify various objects in the retina. samples studied. To evaluate the classification accuracy of the proposed method in terms of discriminating between HE and non-HE pixels, Table 1 shows the values of the dispersion matrix (Jindex) for cluster prominence, characteristics, and sum mean and variance were calculated in both the GLM and the HSL color space. The table also includes calculated metric results for RGB, YLQ, HSL, GLM, YCbCr and Lab color spaces. For this test, 1009 EX and 2095 non-EX pixels were manually selected to analyze the separability of the EX and non-EX pixel classes. The EX training package is taken from the available facts. As can be seen in Table 1, the Cluster Promise feature computed for the GLM color space provides the highest index and is therefore used for optimal segmentation of the retina (especially HE) images.

Table 1. Quantitative index of layered separability of different color models and texture descriptors

Color model	Texture descriptor	Scatter matrix (J)
GLM'	Sum means	5.81
HSL	Sum means	5.4
GLM'	Variance	5.63
HSL	Variance	5.13
GLM'	Cluster prominence	13.6
HSL	Cluster prominence	9.8
GLM'	Sum means	5.81

1.7 Signature maps Analysis

Based on available facts, the best performing feature maps were first selected based on their accuracy in classifying different structures in retinal images. To quantify the accuracy of the classification, a trace index J was determined. It estimates the separability of pixel classes (EX vs. non-EX). To quantify the accuracy of the classification, the trace data were calculated according to Equation (14). The J-metric estimates the separability of pixel classes (e.g., EX vs. non-EX) using intralayer (Sw) and mid-layer (Sb) scatter matrices as follows:

$$J = trace(\mathbf{S}_b \mathbf{S}_w^{-1}) \tag{14}$$

Where: trace is a function which returns the sum of diagonal elements of a square matrix.

$$\mathbf{S}_b = (\mu_{ex} - \mu_{non-ex})(\mu_{ex} - \mu_{non-ex})^T \tag{15}$$

$$\mathbf{S}_w = \mathbf{S}_{ex} + \mathbf{S}_{non-ex} \tag{16}$$

μ_{ex} and μ_{non-ex} are the means of the EX and non-EX classes respectively, estimated using the corresponding training sets.

\mathbf{X}_{ex} and \mathbf{X}_{non-ex} are the training sets for EX and non-EX classes respectively.

N and M are the total numbers of X_{ex} and X_{non-ex} that are present in the training set respectively.

$$\mu_{ex} = \frac{1}{N} \sum_{i=1}^N \mathbf{X}_{ex}^i \tag{17}$$

$$\mu_{non-ex} = \frac{1}{M} \sum_{i=1}^M \mathbf{X}_{non-ex}^i \tag{18}$$

\mathbf{S}_{ex} and \mathbf{S}_{non-ex} are the scatter matrices of each class:

$$\mathbf{S}_{ex} = \frac{1}{N} \sum_{i=1}^N (\mathbf{X}_{ex}^i - \mu_{ex})(\mathbf{X}_{ex}^i - \mu_{ex})^T \tag{19}$$

$$\mathbf{S}_{non-ex} = \frac{1}{M} \sum_{i=1}^M (\mathbf{X}_{non-ex}^i - \mu_{non-ex})(\mathbf{X}_{non-ex}^i - \mu_{non-ex})^T \tag{20}$$

A higher J value means that the classes are more segregated, while the members of each class are closer together. In addition, a series of tests were performed on the resulting signature maps by modifying some parameters of the algorithm. The following cases were investigated:

- Effects of extraction with and without PCA application.
- Effect of applying PCA on the maximum value of the modified image matrix.
- The effect of the positioning window measurement.
- Reduce the background with modifying the size of the window.

In each case, the effectiveness of the resulting signature map was appropriately assessed by quantitatively comparing the signature map to available ground truth values. For normalization, each component (channel) is divided by its maximum. However, the appearance of false peaks or noise signals during this process can suppress the actual image information in the resulting color image. Also, changing these maximums from image to image or on the same image in different areas will cause unwanted color changes in the signature map.

To solve this problem, the value located in the top 95% of the distribution was taken as the nominal maximum. The top 5% of all feature distributions in the feature space were truncated to the maximum, that is, the nominal maximum. Then divide all values by the maximum. To solve this problem, the values in the top 95% of the distribution were taken as their nominal maximums. The top 5% of all feature distributions in the feature space were truncated to the maximum, that is, the nominal maximum. Then divide all the values by the maximum.

1.8 Performance evaluation of the NN in segmenting HEs

Quantitative analysis is carried out to evaluate the performance of the proposed NN in segmenting to detecting HEs from the other structures. For this, a set of tests HE and non-HE pixels taken from different spatial positions, and structures of different sample retinal images were taken. For the sake of performance evaluation, four commonly used metrics were computed: sensitivity, specificity, positive predictive value, and accuracy.

- Sensitivity (SE):** The percentage of true positive outcomes predicted correctly. Sensitivity can be mathematically defined as $SE = \frac{TP}{TP+FN}$; where TP represents true positives (total number of pixels detected by the proposed method while HE was present) and FN represents false negatives. (Total number of pixels detected by the proposed method as non-HE while HE was present).
- Specificity (SP):** This is the proportion of actual predicted to be negative. It can be defined as $P = \frac{TN}{TN+FP}$, where TN represents true negatives (total number of pixels detected as non-HE by the proposed method) and FP is false positive (total number of pixels detected as HE by the proposed method in the absence of HE).

- Positive predictive value (PPV):** Measures the likelihood of an actual positive being predicted positively. It is defined as $PPV = \frac{TP}{TP+FP}$
- Accuracy (ACC):** This is the probability of correctly identifying a person, i.e. the percentage of correct results (positive or negative correction). Calculated as: $ACC = \frac{TP+TN}{TP+TN+FP+FN}$

VI. RESULTS AND DISCUSSION

At each image processing phase results has been collected and evaluated before preceding to the next phase of the image processing. The result found at each phase of the processes is presented and discussed below.

1.9 Results from Signature Map Analysis

Signature maps created with cluster prominence calculated in the GLM color space performed better than other features. Correctly distinguished OD and HE. Even in the case of glaucoma, this feature can be used to successfully localize OD. In the absence of DR, the signing card will place the OD correctly. Fig. 5 shows a calculated feature map of representative fundus images of two patients treated for moderate nonproliferative DR. In each case, HE (white-blue) was correctly identified by the proposed scheme. OD (cyan) was also correctly identified.

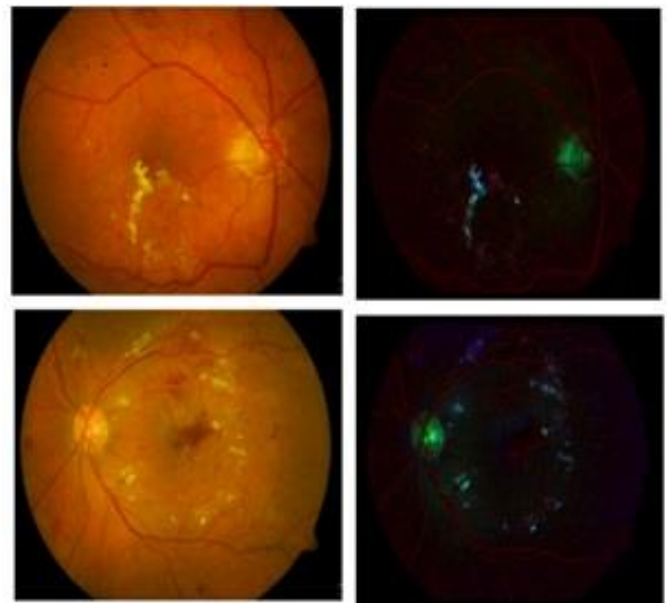


Fig. 5 Original image containing medium non-proliferative DR (1st row) and corresponding signature map (2nd row) created with the proposed scheme.

Fig. 6 shows the results to demonstrate the effectiveness of the proposed program in OD localization. For glaucoma and normal cases, very compact signatures were generated for the OD (cyan), which stood out clearly from the background. At this stage, only qualitative analysis is performed comparing the results of the signature map with the underlying data available.

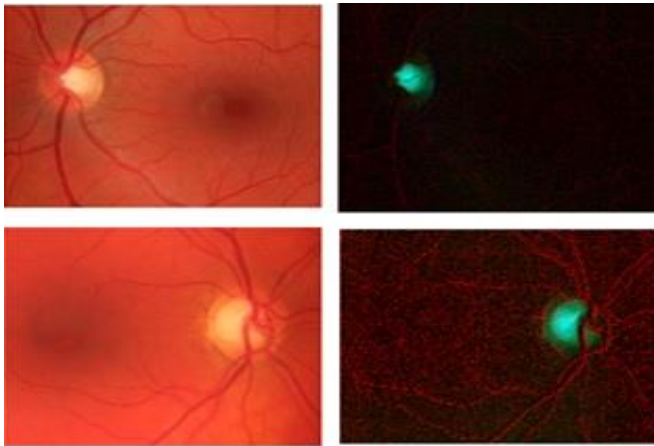


Fig. 6 Original images with moderate non-proliferative DR (1st column) and the corresponding signature cards created with the proposed scheme (2nd column).

The results of the signature tag suggest that the method proposed in this study is capable of identifying secretions. A clear textural feature of these unusual markers was observed in the produced signature maps. In general, there is a good agreement between the generated signature maps and the underlying truth available. Therefore, the proposed multichannel texture map can be used as a powerful tool for image segmentation and classification.

Experiments were performed with 214 retinal stock images. Images were obtained from healthy individuals and patients treated for DR and glaucoma. The test group includes not only good quality images with different background and lighting colors, but also low-quality images due to poor lighting and noise. Experimental tests have shown that the algorithm works best when using a 3x3 rendering window and applying PCA to the TFFT-converted image matrix. The resulting signature map was found to be very useful for visual enhancement of pathological signs with DR, OD localization and EX resistance.

As can be seen in Fig.5, the EX of the generated signature map is displayed in bluish white and contrasts with the background of the other structures and the rest of the background. Signature maps provided significant visual improvement and distinction between HE and OD. A total of 125 DR-induced retinal abnormal images were acquired during the experiment, and the corresponding signature map recognized HE pixels as unique colors. Overall, the robustness of the algorithm to changes in background color and lighting conditions was found to be very satisfactory. Our results showed that the most informative for identifying EX is the third component of the signature map. In addition to visually enhancing HE and OD, signature maps automate the segmentation process by providing critical information that sets thresholds for features that can serve as decision boundaries to differentiate EX from other regions. Experiments have shown that channel 3 provides the highest-grade distinction between HE and OD. The second channel also provides good separation between background pixels and pixels due to HE and OD, but the ability to separate HE and OD is less satisfactory.

1.10 Results of Image Segmentation

The experimental results so far show that the extracted features are very promising in automatic segmentation of HEs, classification of abnormal retinal images based on DR, and visual enhancement of retinal images. The automatic segmentation scheme for HEs proposed in Section IV -C uses an adaptive neural network to detect the presence of exudates (which are the most common markers of DR in the earliest stage) in an image.

Fig.7 HE shows the segmentation results of two representative images with EXs. In both cases, HE was detected very well on each map (pure blue). Results for two retinal images without HE pixels are shown in Fig. 8. In each case, it is clear that the resulting image has no signs of HE (pure blue). In addition to segmentation and classification functions, the proposed method provides improved color contrast for OD and background regions.

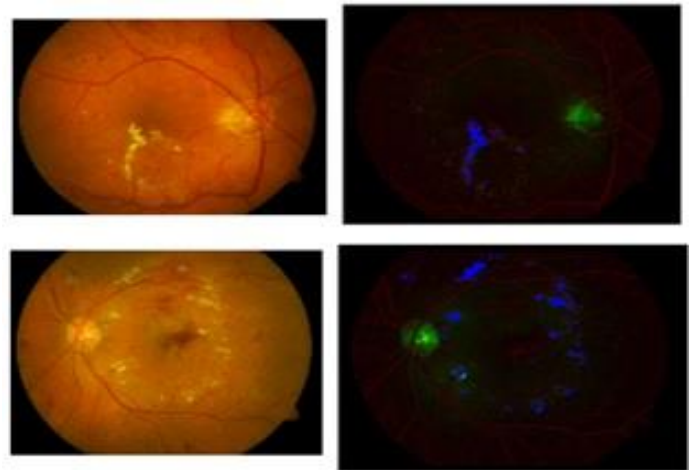


Fig. 7 HE Segmentation results; original retinal images with HE (1st column) and results after segmentation of HE pixels with pure blue color (2nd column).

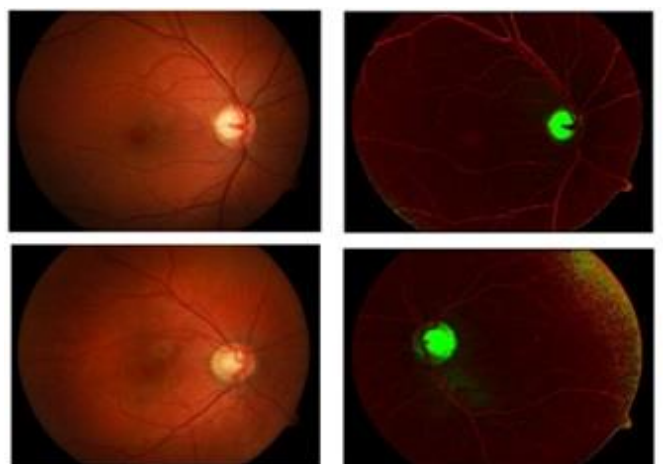


Fig. 8 Results for retinal images containing no exudates; original images (1st column) and results after segmentation (2nd column).

Quantitative analysis was performed to evaluate the performance of the proposed system. For this purpose, two criteria have been established: a pixel-based criterion and an

image-based criterion. The first criterion examines the ability of the proposed algorithm to perform pixel-based detection (i.e. segmentation) of HE, while the second criterion evaluates the ability of the algorithm to distinguish between HE and healthy retinal images. For pixel-based criteria, 64,500 HE pixels from 65 images of retinas with non-proliferative DR and 192,500 pixels without HE (from various anatomical and non-pathological structures) were used. 7 normal images and 30 abnormal images of the retina with H were used as the criteria according to the images. Based on this, the proposed NN-based HE classifier obtained 96.4% SE, 98.7% SP, 96.13% PPV, and 98.12% ACC for pixel-based criteria. For image-based classification, the SE algorithm reached 96.66%, SP 100%, PPV 100%, and ACC 97.3%. In general, it is believed that the clinical use of these systems is acceptable if the SE and SP values are greater than 80% and 90%, respectively. This means that our method is sufficient for clinical use for early detection of exudates.

1.11 Developed User-Friendly Software

To make the application user-friendly and easy to use for the medical personnel, the above image processing algorithm is first built in MATLAB and then it is implemented on C# programming language using Microsoft Visual .Net 2016. The graphic user interface (GUI) developed using C# lets the user to upload the original retinal image and save the processed image result. The user can visualize the stage of the image processing. The user can see RGB retinal image converted to different color space like CMYK, YcbCr and GLM. Some of the Image processing results using the application is shown in the figure below:



Fig. 9 The original RGB retinal image converted to a GLM image



Fig. 10 Image processing result after textural feature extraction



Fig. 11 Applying Artificial neural net to detect the Hard Exudates

VII. CONCLUSIONS

Color retinal image processing employs a three-dimensional representation of color pictures and performs trinion-based Fourier transformations to extract valuable imaging features. The technique also includes a suitable color space transformation, a method for obtaining strong higher-order features, and ANN-based exudate segmentation algorithms. The following two major applications have had their results analysed to illustrate the efficacy of the proposed methods:

- In retinal imaging, visual amplification of the major anatomical and pathological features.
- Automatic HE segmentation and classification of DR anomalies.

The first application explored the potential of signature maps based on multiple higher-order statistical features. A sufficient number of image samples with a wider range of difficulty were used to evaluate the ability of signature maps to extract useful information relevant to DR studies. Priority was the identification of EX and localization of OD. Signature cards were also examined to identify clinically relevant information if glaucoma was present. Texture maps extracted from cluster bump functions and computed in the GLM color space, according to our findings, provide enhanced texture information that can be used to localize OD in the presence of EX, detect HE, and classify retinal abnormalities based on images. Accurate identification of this retinal shape greatly aids the patient's diagnosis and prognosis. With the help of an ANN classifier applied to the acquired texture data, we were able to accurately segment the HE in the background and other bright spots. The performance of the algorithm was evaluated using statistical indicators such as sensitivity, specificity, positive predictive value, and accuracy calculated for both pixel and image criteria. For HE pixel segmentation, the algorithm reached SE 96.4%, SP 98.7, PPV 96.13%, and ACC 98.12%, and for image-based HE anomaly classification, SE 96.66%, SP 100%. , PPV 100% and ACC 97.3%. The results showed that the proposed method works well and has potential for use in intelligent medical systems using computing to detect DR-related eye illnesses.

Although the findings of this study show that the proposed method is effective, there is still room for development in the scheme before it can be implemented in automatic retinal image processing systems. Aside from EXs, other lesion forms considered relevant in DR research include hemorrhages, microaneurysms, and cotton wool patches, and the suggested method should take these structures into account.

ACKNOWLEDGEMENTS

We would like to thank Hawassa University NORD (HU-NORD) coordinating office and Vice President of Research and Technology Transfer Office for supporting and financing this research project. We would also like to extend our gratitude for Black Lion Hospital for providing us different collection retinal image take by digital fundus camera.

REFERENCES

- [1]. Assefa D., Mansinha L., Tiampo K.F., Rasmussen H., and Abdella K.(2011)The trinion Fourier transform of color images, *Sig Proc.* 91(8): 887- 1900.
- [2]. Assefa D., Keller H., Mnard C., Laperriere N., Ferrari R.J., and Yeung I.(2010a) Robust texture features for response monitoring of glioblastoma multiforme on T1-weighted and T2-FLAIR MR images: A preliminary investigation in terms of identification and segmentation, *Med Phys.*, 37(4), pp. 1722-1736.
- [3]. Anup V. Deshmukh, Tejas G. Patil, Sanika S. Patankar, and Jayant V. Kulkarni, Features (2015) Based Classification of Hard Exudates in Retinal Images, *International Conference on Advances in Computing, Communications and Informatics (ICACCI)*, DOI: 10.1109/ICACCI.2015.7275850.
- [4]. Eadgahi M.G. and Pourreza H.(2012) Localization of hard exudates in retinal fundus image by mathematical morphology operations, *Int Conf Comput Knowledge Eng. (ICCKE)*, pp. 185-189.
- [5]. Ehsan S. and Somayeh Z. (2012) Automatic Segmentation of Retina Vessels by Using Zhang Method, *World Academy of Science, Engineering and Technology International Journal of Biomedical and Biological Engineering*, Vol:6, No:12, 2012
- [6]. Godse, Deepali A., and Dattatraya S. Bormane.(2013) Automated localization of optic disc in retinal images. *International Journal of Advanced computer science and Applications* 4.2.
- [7]. John E. Dowling, (2002) *Encyclopedia of the Human Brain*, Volume 4. USA: Elsevier Science.
- [8]. Kande G.B., Subbaiah P.V., and Savithri T.S. (2009) Feature extraction in digital fundus images, *J Med Bio Eng.* 29 (3):122-130.
- [9]. Liu C., Lu H., Zhang J. (2008) Using Fast Marching in Automatic Segmentation of Retinal Blood Vessels. In: Peng Y., Weng X. (eds) *7th Asian-Pacific Conference on Medical and Biological Engineering. IFMBE Proceedings*, vol 19. Springer, Berlin, Heidelberg. <https://doi.org/10.1007/978-3-540-79039-660>.
- [10]. Lu H. and Fang G. (2013) an effective framework for automatic Segmentation of hard exudates in fundus images, *J Circuit Syst Comp.*, 22(1).
- [11]. M. Afzal Mir,(2003) *Atlas of Clinical Diagnosis*, SAUNDERS, Elsevier Science Limited, 2nd ed.
- [12]. Niemeijer M., Ginneken B.V., Russell S.R., Suttorp-Schulten A., and Abramoff M.(2007) Automated detection and differentiation of drusen, exudates, and cotton-wool spots in digital color fundus photographs for diabetic retinopathy diagnosis, *Invest. Ophthalmol. Vis. Sci.*, Vol. 48, pp. 2260-2267.
- [13]. Osareh, A. and B. Shadgar (2009) AUTOMATIC BLOOD VESSEL SEGMENTATION IN COLOR IMAGES OF RETINA, *Iranian Journal of Science & Technology, Transaction B, Engineering*, Vol. 33, No. B2, pp 191- 206.
- [14]. Phillips R., Forrester J. and Sharp P.(1993) Automated detection and quantification of retinal exudates, *Graefes Arch. Clin. Exp. Ophthalmol.* 231(2): 90-94.
- [15]. R. VIKRAM, P. RAJESH, DISEASE DIAGNOSIS USING RETINAL IMAGE PROCESSING THROUGH NEURAL NETWORKS, *International Journal of Grid and Distributed Computing*, Vol.13, No.1, 2020, pp. 76-85.
- [16]. Satya B., Abhay K.(2019) Detection of Hard Exudates in Retinopathy Images, *Advances in Distributed Computing and Artificial Intelligence Journal*, Vol.8 N.4, 41-48, DOI: <http://dx.doi.org/10.14201/ADCAIJ2019844148>
- [17]. Shengchun L., Xiaoxiao H., Zhiqing C., Shahina P., Dingchang Z. (2019) Automatic Detection of Hard Exudates in Color Retinal Images Using Dynamic Threshold and SVM Classification: Algorithm Development and Evaluation, *BioMed Research International*, Article ID 3926930, 13 pages, <https://doi.org/10.1155/2019/3926930>
- [18]. SHILPA JOSHI and P. T. KARULE, (2018), Detection of Hard Exudates Based on, Morphological Feature Extraction, in *Biomedical & Pharmacology Journal*, Vol. 11(1), pp. 215-225.
- [19]. Snchez C., Garca M., Mayo A, Lpez M., and Hornero R.(2009) Retinal image analysis based on mixture models to detect hard exudates,, *Med Image Anal.*, 13(4):650-658.